IS-PORTO 2023 PROCEEDINGS

Proceedings of the 8th International Symposium on DEFORMATION CHARACTERISTICS OF GEOMATERIALS Porto, 3rd - 6th September 2023

Diatoms microfossils and their microstructural effects on the sensitivity of metastable silty-clayey soils

Elaine Barreto[1#], *Tácio M.P.* de Campos[1] and *Sandro S.* Sandroni[1]

[1] *Pontifical Catholic University of Rio de Janeiro, Department of Civil and Environmental Engineering, Rio de Janeiro, Brazil*

[#]*Corresponding author: elainebarreto@id.uff.br*

ABSTRACT

In 2013, an accident occurred in Port of Santana, located at the mouth of the Amazon River, in the State of Amapa, Brazil, comprising a large volume of soft silty-clay soil flowing very fast, for a great distance, towards the bottom of the river. Field tests performed afterwards identified the occurrence of sensitive soil layers at the site. Subsequent laboratory tests verified the presence of diatom microfossils in layers with highest liquidity indices. Owing to peculiarities of the accident, a large research programme started at PUC-Rio, aiming to investigate the role of these biomineral grains on soil behaviour. Thus, based on physical-chemical-mineralogical tests performed on samples from the site, higher sensitivity natural soils from Port of Santana were reconstituted. Chemical, mineralogical and grain size reconstitution was carried out using manufactured soils containing equal proportions of minerals as in the natural soils, but with a difference in the portion of non-plastic siliceous grains: a reconstituted soil used quartz, in silt size, and the other used diatomaceous earth. This article presents and discuss results of undrained shear strength data obtained through laboratory fall cone and vane tests, as well as microstructure analyses - including scanning electron microscopy, mercury intrusion porosimetry and X-ray microtomography - in high sensitivity natural diatomaceous soils and reconstituted soils, in the liquidity index range of $1.0 \leq LI \leq 1.6$. It is shown the fundamental role of the diatom microfossils in microstructural metastability, impacting the high sensitivity measured in soil reconstituted with diatoms and in natural diatomaceous soils.

Keywords: diatom microfossils; microstructure; metastable soft soil; laboratory tests.

1. Introduction

In 2013 occurred an accident at the Port of Santana, in the State of Amapa, Brazil, in which a large volume of soft silty-clay soil flowed for a large distance, towards the bottom of the Amazon River. After the failure, field investigations identified the occurrence of sensitive soil layers at the site, through CPTU tests (Sandroni et al. 2015). Analysing images of scanning electron microscopy (SEM) of samples of this geological material, Barreto (2015) identified the presence of diatom microfossils in those showing the highest liquidity indices (LI). Low undrained remoulded strengths (s_{ur}) and high sensitivities (S_t) were identified through fall cone tests, mainly in soils with the highest concentrations of diatom microfossils.

Diatoms are microscopic algae that, after death, fossilize due to the adsorption of silica dissolved in the water they are in, biomineralizing as a quartz polymorphism and forming the skeletons of silica microfossils that sediment together with mineral particles of clayey soil, forming a structured clay material.

Soil structure is an important aspect of the geotechnical behaviour of clays with high water content. Alteration or collapse of the clay structure is often mentioned to account for many aspects of the mechanical behaviour of structured clays. To evaluate the pores network preserving the initial soil structure, with minimum perturbation, it has been used the lyophilization technique, in which the samples are prepared by quick freezing in liquid nitrogen and drying under vacuum (Delage and Lefebvre, 1984).

Collins and McGown (1974) studied the microfabric of various normally and slightly overconsolidated clays using SEM and classified the pore spaces into four broad groups: intra-elemental, intra-aggregate, inter-aggregate, and trans-aggregates, with the intra- and inter-aggregate terms being the most used in the literature. Tanaka and Locat (1999), studying the microstructure of Asian fossiliferous clays, introduced the terms skeletal and intraskeletal porosity to describe the pore network associated with the presence of microfossils. Locat and Tanaka (2000, 2001) suggested the classification of pore families into four groups: inter-aggregate, the pore space between particle aggregates; intra-aggregate: the pore space internal to the aggregates; skeletal, the pore space referring to the chambers in the wall of the microfossil's frustule, and intra-skeletal, the pore space within the microfossil skeleton.

The mercury intrusion porosimetry (MIP) technique has been used to examine the microstructure of soils and can provide quantitative information about the distribution of pore throat sizes within the material. Mercury porosimetry is based on the principle that a non-wetting fluid such as mercury does not enter the porous medium unless pressure is applied. The pores are compared to capillary cylinders and the applied pressure, P, is related to a pore entry radius, r, through the Washburn (1921) equation commonly referred to as Laplace's Law (Delage and Lefebvre, 1984), which is

presented in equation 1, where σ is the surface tension of mercury and θ is the solid-liquid contact angle:

$$P = 2\,\sigma \cos\theta / r \quad (1)$$

Diamond (1970) was the first to investigate the pore size distribution of clays using MIP analysis, measured contact angles for different clay minerals and indicated θ = 147° for kaolinite and illite in contact with mercury. Delage and Lefebvre (1984) used a combination of SEM and MIP results to describe the microstructure of the sensitive clay from St Marcel de Champlain, Canada, in undeformed and dented states and at different levels of densification. They showed that the clay consolidation results in the collapse of its inter-aggregate pores, leaving its intra-aggregate pores almost intact. Tanaka et al. (2001) used SEM images to illustrate the flocculated and metastable structure of the diatom fossiliferous quick clay from Ariake Bay, Japan. Hong et al. (2006) also used SEM and MIP analysis to evaluate changes in the microstructure of the natural diatomite from Oita, Japan, under consolidation. Sasanian and Newson (2013) used MIP to investigate the microstructures of reconstituted clays.

According to Tanaka and Locat (1999), the skeletal pore space is easily recognized in a logarithm-differential pore distribution curve of MIP as a set of micropores with a radius ranging from 0.02 to 0.1 μm. With image and pore measures, the classification of pore families can be summarized as (1) Inter-aggregate: pores have different sizes, are larger than 2 μm, and can have dimensions of tens of micrometres; (2) Intra-aggregate: pores are smaller than 0.5 μm; (3) Skeletal: varying in diameter, but usually smaller than 1.0 μm in the frustule; (4) Intra-skeletal: diameter between 40 μm and 60 μm and distinguishable by their rounded shape.

The X-ray microcomputed tomography (micro-CT) presents itself as a non-destructive radiographic imaging technique to characterize the internal microstructure of material in three dimensions at the micron-level spatial resolution, with minimal sample preparation (Landis and Keane, 2010). This technique has the limitation of the tomographic resolution, which influences the smaller visualized pore by the defined pixel size (which must be greater than 0.5 μm).

Effects of diatom microfossils on the development of clayey soils of high sensitivity have been investigated through mineralogical and grain size reconstitution of the higher sensitivity natural soils of Port of Santana (PS) and through sensitivity and microstructural tests (Barreto 2021). In the present paper, results of laboratory fall cone and vane tests, as well as microstructure analysis - including SEM, MIP and micro-CT – performed in high sensitivity natural diatomaceous soils and on quartzose (SRQ) and diatomaceous (SRD) reconstituted soils, at a liquidity index range of $1.0 \leq LI \leq 1.6$, are presented and discussed.

2. Materials and Methods

2.1. Reconstitution method

After mineralogical analysis of the Port of Santana soils via DRX (powder method) and quantification via Rietveld's (1966) method, chemical, mineralogical and granulometric reconstitution was carried out using four manufactured materials: kaolin and illitic green clay - containing the same clay minerals as natural PS soils -, quartz and diatomaceous earth (see Figure 1) – both non-plastic siliceous particles, in silt size. The quantity of manufactured soils in the mixtures was determined to also reproduce the granulometric curve of the natural soil, using 25% of kaolin, 35% of green clay and, in the other 40%, non-plastic siliceous grains: one using quartz forming the SRQ soil, and another using diatomaceous earth (commercial name) forming the SRD soil.

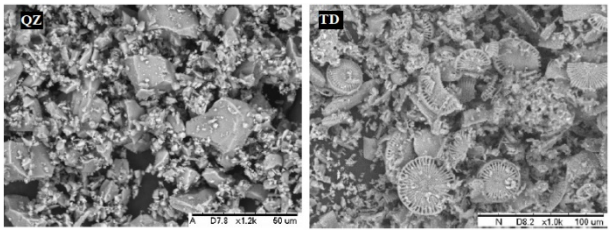

Figure 1. SEM images of manufactured siliceous materials – QZ and TD. (aumentar QZ e TD na figura)

2.2. Geotechnical characterization of natural and reconstituted soils

Table 1 presents geotechnical characteristics of the sensitive diatomaceous natural soils of Port of Santana and of the reconstituted soils, defined following Brazilian standards, which are equivalent to respective American standards.

The natural soils taken from different depths (36 and 38 m) are similar to each other, being classified as MH (USCS). Soil PS 1A 38 m has, however, a higher concentration of microfossils, demonstrated by its higher natural water content and higher liquidity index.

Table 1. Geotechnical characterization of reconstituted and natural soils.

Soil	G_s	Sand %	Silt %	Clay %	w_L %	w_P %	PI %	w_n %	LI	USCS	Ac
PS 1A 36 m	2.63	3	57	40	50	33	17	55	1.3	MH	0.4
PS 1A 38 m	2.63	3	62	35	61	42	19	82	2.1	MH	0.5
SRQ	2.65	5	52	43	42	20	22	-	-	CL	0.5
SRD	2.52	6	55	39	59	36	23	-	-	MH	0.6

G_s = grain density by the pycnometer method; w_L = liquid limit; w_P = plastic limit, both without prior drying, the first using the Casagrande device; PI = plasticity index; w_n = natural water content; LI = liquidity index; USCS = Unified Soil Classification System; Ac = colloidal activity.

The reconstituted SRD soil has a lower grain density, G_s, than the SRQ since the diatom microfossil grain is very porous and less silicified and, therefore, less dense than the quartz grain. The SRD showed an increase in w_L and w_P of about 17 % in relation to the SRQ. This means that, at the liquid limit, microfossils store 29 % of the total water in the soil inside their skeletons, due to physicochemical phenomena of water adsorption to the surface of their electrically charged frustules. Although SRQ and SRD have similar PI and colloidal activity, they are classified differently on the Casagrande plasticity chart because of the effect on w_L.

Comparing the natural diatomaceous soils with the reconstituted SRD, they are similar, being classified as MH. The only relevant difference among them is the Gs value, smaller in the case of the reconstituted soil. This indicates that the natural diatomites are denser than the industrialized one. Their capacity of water retention is, however, similar. Indeed, if this capacity, which is reflected in their higher liquid limit, were not considered, both the natural and the SRD soils would be better classified as CL in the USCS.

2.3. Fall cone and vane laboratory tests

To evaluate the undrained strength, s_u, of PS soils it was used a Geonor fall cone equipment. Succinctly, in this equipment, one of four metallic cones is chosen based on its mass, cone tip angle and the consistency of the soil, to free fall on the surface of the soil sample, taking the penetration value. The calibrations of the cone characteristics and the penetration in the soil sample are related to the obtained s_u value.

Pieces of Shelby tubes with a diameter of 7.5 cm were cut to a height of 5.0 cm, and PS samples were tested in the laboratory to obtain sensitivity using determinations of s_u in the intact sample and the remoulded undrained strength, s_{ur}, in the sample manually remoulded by squeezing in a closed plastic bag to avoid loss of water content.

Tanaka et al. (2012) used the fall cone to measure the undrained shear strength of Japanese soft clay materials and correlated the results with those of other s_u measurement techniques (field and laboratory vane and UU triaxial tests), showing the validity of the results obtained with this equipment and the ability to obtain smaller s_{ur} by squeezing than after vane turns.

For the reconstituted soils, SRQ and SRD, individual saturated samples of soils were prepared adding deionized, distilled water to each initially air-dried material up to reaching a water content equal to 1.4 w_L. After throughout homogenization with a spatula, the slurries were left to rest for a minimum of 24 hours for moisture equilibrium. Measures of moisture content of subsamples from the after-rest slurry did not indicate any segregation condition in the prepared slurry. Then, the slurry was placed directly into the consolidation ring, taking care to avoid the occurrence of air bubbles in the process. Specimens, with measured total mass, were prepared at the same initial water content, and then consolidated to different liquidity indices, LI, (or void ratios), in PVC rings of 95 mm in diameter and 60 mm in height.

Undrained shear strength tests were carried out on laboratory vane equipment from Wykeham Farrance, with an electric motor with a standard rotation speed of 11 degrees per minute. The laboratory vane used has blades in a cruciform format 1:1 (H = D), with the geometric parameter K = 4.447 x 10^{-6} m³ and an area ratio of 11.2%.

Maximum undrained strength, s_u, was obtained using equation 2, where b is the calibration parameter of the spring used.

$$s_u[\text{kPa}] = \frac{spring\ deflection\ x\ b}{K} = \frac{torque\ [Nm]}{1000K\ [m^3]} \qquad (2)$$

Remoulded undrained strength, s_{ur}, was obtained by performing the test in three different ways: (i) after 10 manual rotations of the blade at the end of the determination of maximum undrained strength (10 R); (ii) after manual remoulding by squeezing, with the fingers, the sample placed inside a plastic bag sealed against moisture loss (M); (iii) after 10 rotations of the vane in the previously manually remoulded sample (M + 10 R).

2.4. SEM images

SEM images were made aiming at the characterization of microstructure and pore families. A JEOL JSM-6510LV low vacuum SEM from Thermo Scientific was used for PS soils, and a TESCAN CLARA system, with high resolution, was used for the characterization of SRQ and SRD soils.

Specimens of PS soils were initially in their natural consistency and the reconstituted soils were extracted from the consolidated specimens prepared for the laboratory vane tests, up to different levels of effective stress - SRQ (LI = 1.0) and SRD (LI = 1.2). For all of them, it was performed the extraction of specimens by cutting with fine metallic wire, in a prismatic shape of 0.5 x 0.5 x 1.0 cm of size, in vertical and horizontal planes of soils.

Due to the limitation of the equipment used for microstructural evaluation in not analysing very wet samples and the need to visualize the soil structure with as little disturbance as possible, it was necessary to apply the freeze-drying (lyophilization) technique, which consists of instantly freezing the soil by submerging it in liquid nitrogen (temperature -170°C), abruptly fragment the specimen into a view plane and then dry it by sublimation of ice using a vacuum desiccator, for at least 6 hours, depending on each soil. And finally, the specimens were metallized with gold, to improve conductivity and image quality.

2.5. MIP curves

MIP analysis were performed in an Autopore 9320 porosimeter, from Micromeritics, on PS and consolidated specimens of SRQ (with LI = 1.0) and SRD (with LI = 1.2), with prismatic shape with approximately 1.0 x 1.0 x 1.5 cm of size, dried by lyophilization.

The porosimeter has the following operational characteristics: pore size distribution: 197 – 0.006 μm, low pressure up to 26 Psi (180 kPa): 197 – 6.9 μm, high pressure up to 29,471 Psi (203 MPa): 6.9 – 0.006 μm. In

the tests, the following parameters were considered: contact angle of 130° and mercury surface tension of 485 N/mm. The test procedure consists of placing the sample inside the glass chamber of the penetrometer where it is subjected to a vacuum pressure of 50 µmHg for 15 minutes, whose objective is to remove air and fill the capillary tube with mercury. Low levels of pressure are applied to envelop the entire surface of the sample with mercury. Then the sample is subjected to increasing pressures. At each stage, a period of 30 seconds is necessary for the stabilization of the applied pressure and the volume of injected mercury is recorded. Such volume it considered to correspond to the interconnected pore volume of the soil.

2.6. Micro-CT images

To perform 3D imaging of the soil samples it was used an Xradia Versa XRM-510 high-resolution X-ray micro tomograph, from ZEISS. Specimens were prepared like the SEM, with a prismatic shape of approximately 0.5 x 0.5 cm in cross-section and variable height, and freeze-dried.

The image acquisition recipe was: 4x objective lens; source distance = 40 mm; detector distance = 110 mm; voxel size = 0.9 µm; BIN 1; exposure time = 17 seconds/projection; 1600 projections. Source voltage = 160 kV, power = 10 W and current = 62.4 µA.

When evaluating micro-CT images, it should be borne in mind that the greater the attenuation of X-rays (reduction of the intensity of an X-ray beam as it traverses matter), the brighter is the object in the image (Landis and Keane, 2010). Thus, pores are recognized as the darkest objects and, after contrast expansion, quartz grains are medium grey, feldspars and kaolinite clay are light grey and particles containing iron in the composition (oxides or illite, for example) are whitish.

To get an overview of the 3D microstructure the micro-CT images were analysed in cubic interest volumes of 1000 voxels³ and 900 µm on sides. To extract the total visible porosity attribute, the volumes were segmented into pores and mineral phases by the *Fiji ImageJ* program using a machine learning tool (Staniewicz and Midgley, 2015) named *Trainable Weka Segmentation* plugin (Arganda-Carreras et al., 2017).

3. Sensitivity Results

Figure 2 presents examples of results of laboratory vane tests performed on SRQ consolidated at σ'_v = 20 kPa (LI = 1.0) and on SRD consolidated at σ'_v = 80 kPa (LI = 1.2). It can be seen in Figure 2 that the SRD has undrained shear strength, s_u, eight times higher than the SRQ, even being under a higher LI.

It is important to note here that, at the effective consolidation stress of σ'_v = 80 kPa, the SRQ soil presented a LI = 0.8 (so, out of the range of LI herein considered) and a lower undrained shear strength (s_u = 12 kPa), showing that the higher undrained shear strength of SRD is an intrinsic characteristic promoted by the presence of the diatom microfossils on the soil and not by the structure reached after consolidation.

Still in Figure 2, concerning the remoulded undrained shear strength, s_{ur}, the difficulty of obtaining the minimum s_{ur} is greater in the SRD. The s_{ur} mechanically obtained after 10 turns with vane (10 R) is about 4 times greater than the minimum s_{ur} obtained after manual remoulding by squeezing plus 10 turns with vane (M + 10 R). This indicates that the disturbance effort capable of making the soil reach its minimum s_{ur} and releasing the water contained within the microfossils requires both squeezing remoulding and vane revolutions. Such differences in s_{ur} values have a great impact on S_t calculation (Barreto 2021).

To evaluate the influence of the intrinsic undrained shear strength and the variation of the remoulding technique, Figure 3 illustrates sensitivity measures on specimens of both reconstituted soils prepared by consolidation up to various liquidity indices.

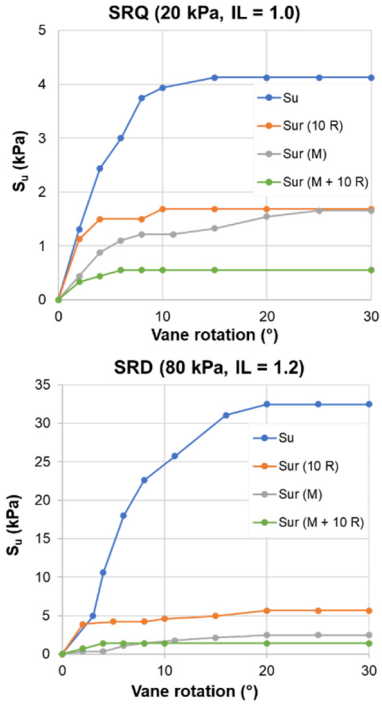

Figure 2. Laboratory vane results of SRQ e SRD soils.

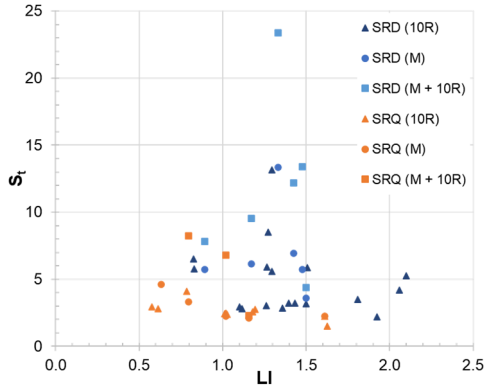

Figure 3. S_t x LI x s_{ur} relations of SRQ and SRD.

For the SRQ in Figure 3, it is observed that in the interval of 1.0 ≤ LI ≤ 1.6, in which there would be a possibility of a flowslide in the field (Lebuis et al., 1983), the measured intrinsic S_t are in the interval between 2 and 7, indicating that this soil does not exhibit metastability.

In the case of the SRD, the effects of structural metastability and potential for flowslide, intrinsic to the presence of diatom microfossils, are shown in Figure 3 in the range of $1.1 \leq LI \leq 1.6$ when it is used s_{ur} (M) and, mainly, s_{ur} (M + 10 R), with sensitivity varying between 6 and 22.

The percentage of remoulding loss, defined by Skempton and Northey (1952) by equation 3:

$$\frac{s_u - s_{ur}}{s_{ur}} \, x \, 100 \, \% \qquad (3)$$

is more expressive on SRD soil, even considering just the s_{ur} (10 R).

Table 2 presents a summary of undrained shear strengths, sensitivity and percentage of remoulding loss results on selected specimens submitted to microstructural analysis.

Table 2. Summary of laboratory vane and fall cone test results on selected specimens.

Specimens	LI	s_u (kPa)	s_{ur} (10 R) (kPa)	S_t	$\frac{s_u - s_{ur}}{s_u}$ (%)	s_{ur} (M) (kPa)	S_t	$\frac{s_u - s_{ur}}{s_u}$ (%)	s_{ur} (M+10 R) (kPa)	S_t	$\frac{s_u - s_{ur}}{s_u}$ (%)
SRQ (LV)	1.0	4.1	1.7	2	58.5	1.6	3	61.0	0.6	7	85.4
SRD (LV)	1.2	33.0	6.0	6	81.8	2.5	13	92.4	1.5	22	95.5
PS 36 m (FC)	1.3	49.0		-		2.1	23	95.7		-	
PS 38 m (FC)	2.1	27.0		-		1.7	16	93.7		-	

LV = laboratory vane test; FC = fall cone test.

4. Microstructural Results

Figure 4 illustrates the microstructural characteristics of PS 1A 36 m soil with SEM images.

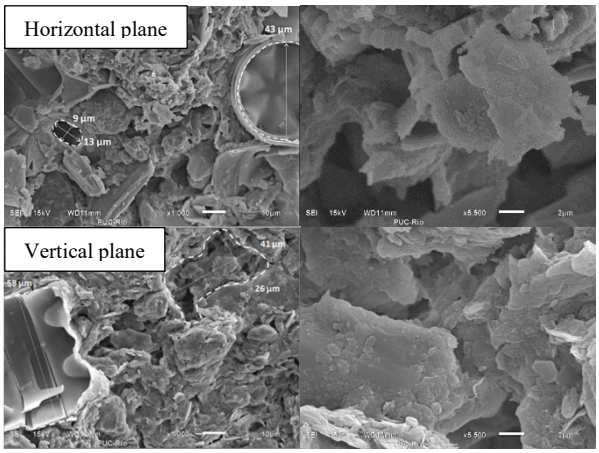

Figure 4. SEM images of PS 1A 36 m (LI = 1.3, e = 1.45).

It can be seen in Figure 4 that the PS 1A 36 m soil presented a non-oriented clay matrix randomly mixed with coarse silt-sized particles, including primary minerals, microfossils of whole diatoms and their fragments, in a bidirectional flocculated arrangement. It presented the four families of pores: intra-aggregate, inter-aggregate, skeletal and intra-skeletal. Intra-aggregate pores are those smaller than 0.5 µm, some being visualized at the highest magnification. The inter-aggregate pores have different sizes, most of them are larger than 2 µm, and some large pores with dimensions of about 40 µm were observed. As for the intra-skeletal pores, some tubular with a dimension of 10 µm were observed, others in the circular and whole centric microfossils with a diameter of around 40 µm, and also in the fragments of these fossils with dimensions of about 60 µm. Skeletal pores had different diameters, from 0.3 µm in the frustule of the whole diatom to almost 1.0 µm in fragments of tubular microfossils.

Figure 5 illustrates the microstructural characteristics of PS 1A 38 m soil with SEM images.

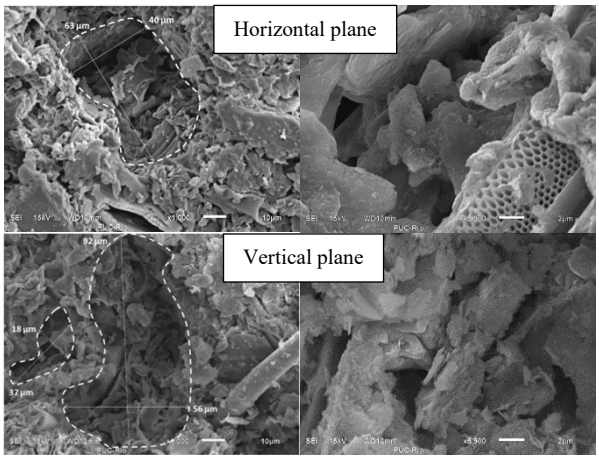

Figure 5. SEM images of PS 1A 38 m (LI = 2.1, e = 2.15).

It can be seen in Figure 5 that the soil PS 1A 38 m has the most flocculated, open and porous microstructure of all, containing less aggregated clay matrix, coarse mineral grains and many whole and fragmented microfossils arranged randomly. At the highest magnification, clay particles and some small microfossil fragments can be seen forming flakes that are associated with each other at the edges, with bridges at close contact. It presented four families of pores: intra-aggregate, inter-aggregate, skeletal and intra-skeletal. Skeletal pores are about 0.3 x 0.7 µm and intra-skeletal pores have varying sizes reaching up to 60 µm. The inter-aggregate pores have different sizes, in the order of 1 µm between clay flakes and up to 90 µm in large macrospores formed between groups of particles. A greater diversity of diatom microfossil species was observed, with different sizes and formats: tubular with 6 µm in diameter and 20 µm in length, in the shape of a circular disk, with a diameter of about 40 µm, frustule thickness of 2 µm and internal pore about 5 µm thick, and in the shape of a wheel.

Figure 6 illustrates the microstructural characteristics of SRQ soil with SEM images.

It can be observed in Figure 6 that the SRQ presented a compact microstructure formed by a non-oriented clay matrix and coarse grains of quartz and feldspar, in silt and fine sand size. It presented two families of pores: intra-aggregate and inter-aggregate. The associations between

clay particles form face-to-face aggregates and these aggregates bond to each other at the edges, forming flakes and composing an aggregate-flocculated but compact microstructure. When they are in a clay matrix, the inter-aggregate pores are from 0.5 to 2 µm.

Figure 7 illustrates the microstructural characteristics of SRD soil with SEM images. It can be seen in Figure 7 that the SRD presents a flocculated and macroporous microstructure, formed by several microfossil particles of whole centric diatoms, with different diameters and thicknesses, arranged in a disorderly way with a flocculated clay matrix and coarse particles of primary minerals. It presented four families of pores: intra-aggregate, inter-aggregate, skeletal and intra-skeletal. It is also observed between the clay particles essentially edge-to-face bonds with some face-to-face aggregation, with narrow contact points and more intra-aggregate porosity, with the effect of cementation with silica between the clay particles, best viewed at higher magnification. Between the aggregates and the microfossils, macropores with an equivalent diameter of 5 to 10 µm are formed. It is also possible to see a solid framework between the skeletons, primary mineral grains and clay flakes cemented by free silica, and the interlocking in this framework forms macropores with sizes from 10 to 50 µm.

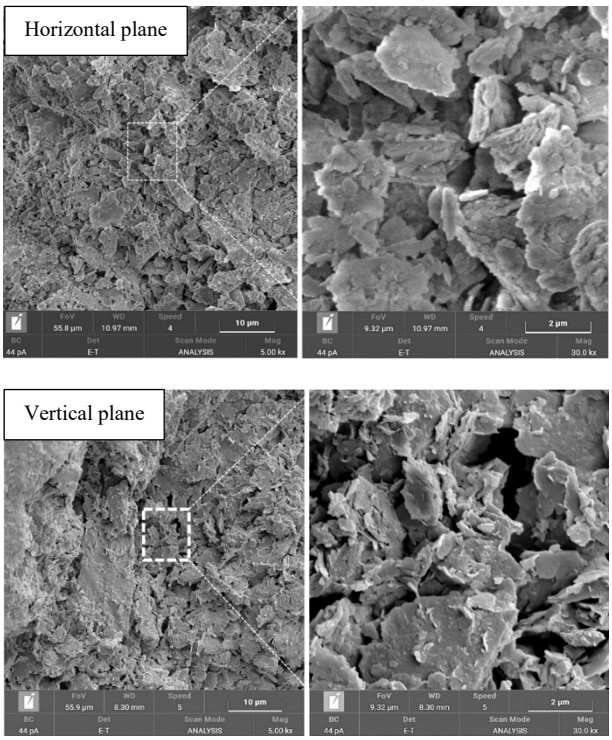

Figure 6. SEM images of SRQ consolidated up to 20 kPa (LI = 1.0, e = 1.11).

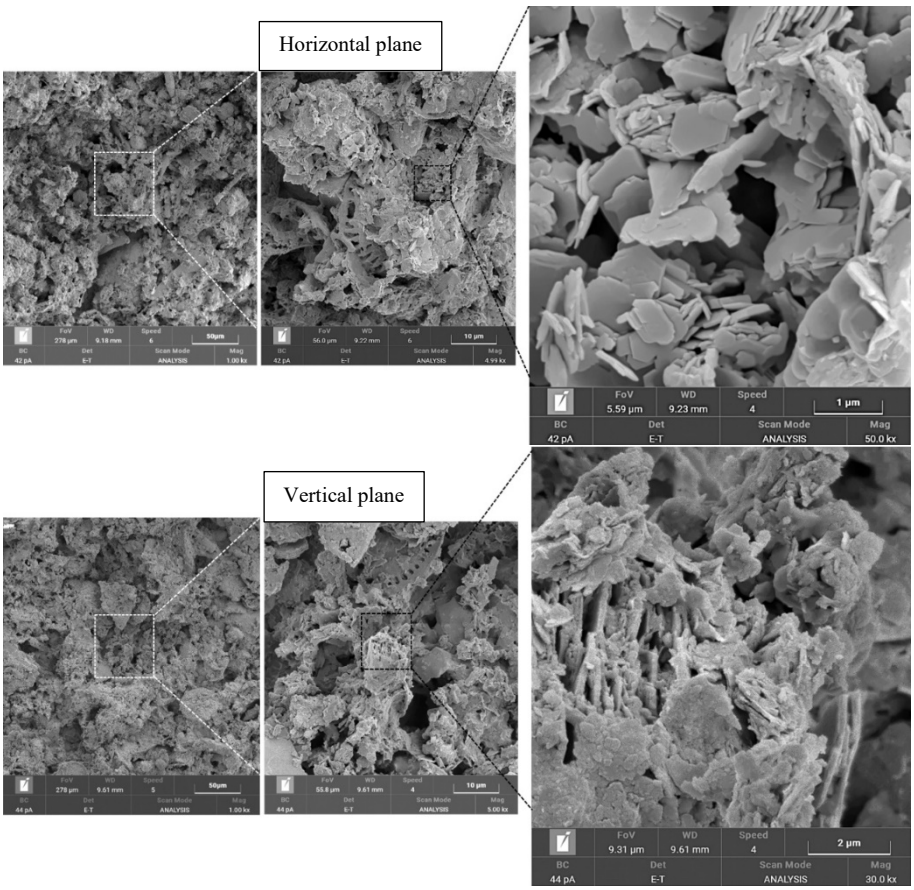

Figure 7. SEM images of SRD consolidated up to 80 kPa (LI = 1.2, e = 1.60).

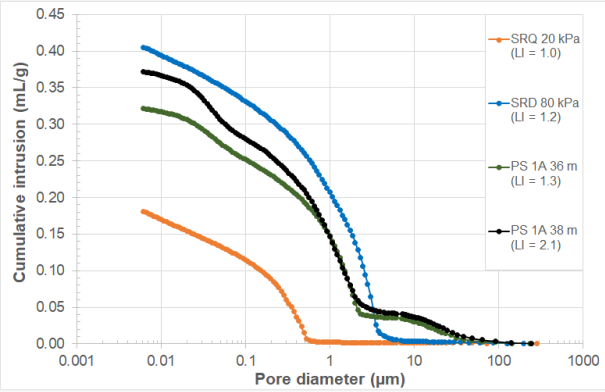

Figure 8. Cumulative intrusion pore distribution curve of MIP.

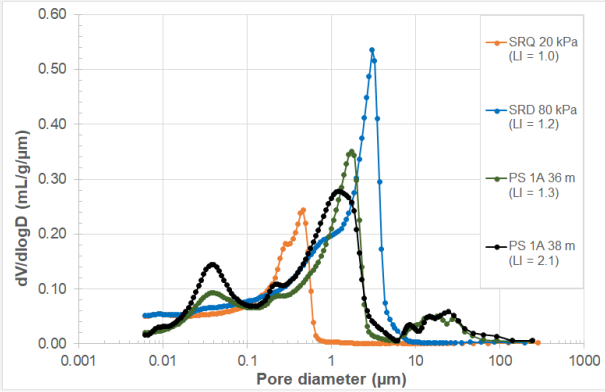

Figure 9. The logarithm-differential pore distribution curve of MIP.

Table 3. Summary of microstructural parameters of MIP results.

Parameter	SRQ	SRD	PS 1A 36 m	PS 1A 38 m
Total intrusion volume (ml/g)	0.18	0.41	0.32	0.37
Total pore area (m^2/g)	15.78	16.87	12.29	15.41
Median pore diameter (volume) (D_{50}, µm)	0.19	1.04	0.84	0.67
Average pore diameter (4V/A, µm)	0.05	0.10	0.10	0.10
Bulk density at 10.55 kPa (g/cm^3)	1.76	1.13	1.32	1.23
Apparent (skeletal) density (g/cm^3)	2.57	2.10	2.28	2.26
Porosity from MIP (%)	31.8	45.9	42.3	45.6
Porosity from physical indices (%)	52.6	61.5	59.2	68.3

Figures 8 and 9 present the pore throat distribution curves of MIP of selected specimens and Table 3 presents a summary of the main microstructural parameters obtained from MIP results.

Observing Figures 8 and 9, it is noted that the SRQ reconstituted soil presented a unimodal pore diameter distribution curve and pores distributed mainly in the range of 0.1 to 0.6 µm, corresponding to intra-aggregate and inter-aggregate porosity. Evaluating the results of Table 3, it is observed that this soil has a more compact microstructure than the others, with a small median pore diameter of 0.2 µm and porosity of 31.8 %.

The SRD reconstituted soil also presented a unimodal distribution curve (with a peak in the pore diameter range of 2 to 5 µm) to slightly bimodal (with a band in the range of 0.5 to 2 µm). There is no clear distinction in the curves of skeletal and intraskeletal pores, which could be explained by the geometric characteristics of the TD grains used in the mixture (see Figures 1 and 7), in which the intraskeletal pores are less expressive than those of diatom microfossils from the natural soils of PS and, sometimes, they are confused with the skeletal porosity of the frustule itself (skeleton wall). However, there is a clear effect of increasing the total porosity (46 %) and the median pore diameter to 1.0 µm.

Both natural, undisturbed soils PS 1A 36 m and PS 1A 38 m showed three-modal pore diameter distribution curves, with a mode with a peak in the range of 0.01 to 0.1 µm, characteristic of the skeletal microfossil pores and intra-aggregate pores, a mode with a peak at approximately 2 µm, corresponding to inter-aggregate pores, and another mode with a peak in the range of 8 to 100 µm, corresponding to intra-skeletal pores and inter-aggregate macropores. In Table 3, it is observed that these soils presented a more macroporous structure, with larger median pore diameters, lower apparent density and porosity between 42 and 46 %.

Regardless the difference in the pore size distribution of the reconstituted soils (unimodal) and of the natural soils (three-modal), there are important similarities in the microstructural parameters of the fossiliferous soils, PS, and the SRD soil. Both materials show greater median pore diameter, lower apparent density, greater intruded volume and greater porosity than that observed in the SRQ soil, demonstrating that such effects arise from the presence of the diatom microfossils. Also, the MIP method presented a porosity difference of around 20 % in relation to that estimated by the physical indices, due to the microporosity that is not reached by the range of mercury injection pressure.

Figures 10, 11, and 12 illustrate 3D microstructures of microtomographed soils PS 1A 36m, PS 1A 38m, and SRD, respectively, where axis are in microns and the z-direction represents the vertical direction.

Overall, the PS 1A 36 m soil microstructure is disoriented and has mixtures of clay matrix, many coarse mineral grains, and diatom microfossils. As the grains of diatom microfossils are porous, the skeletal pores are smaller than the resolution of 0.9 µm and the images are filtered to reduce noise, it is only possible to visualize the contours of the microfossils on micro-CT.

The PS 1A 38 m soil microstructure is also flocculated, disoriented, and has mixtures of clay matrix, coarse mineral grains, and diatom microfossils. Relating to PS 1A 36m, it has fewer quartz and feldspar grains and more centric diatom microfossils, visualized by a large amount of sub-rounded intra-skeletal pores. The intra-skeletal pores are numerous, are very close to each other, and give this sample a “Swiss cheese” appearance. Distributed white point objects are also observed in both samples, indicating cementation with iron oxides. The macropores are interconnected and cemented, forming caves organized to create a skeletal framework that supports the permanence of inter-aggregate macropores.

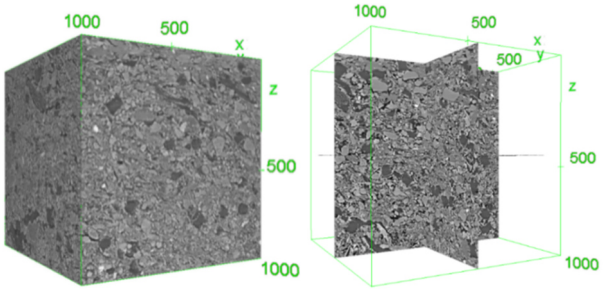

Figure 10. Micro-CT PS 1A 36 m (LI = 1.3, e = 1.45).

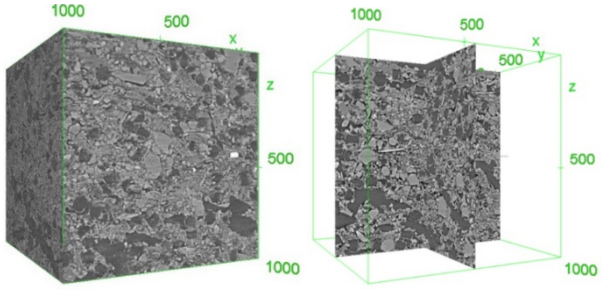

Figure 11. Micro-CT PS 1A 38 m (LI = 2.1, e = 2.15).

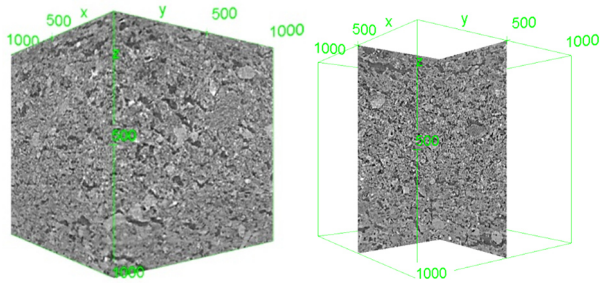

Figure 12. Micro-CT SRD 80 kPa (LI = 1.2, e = 1.60).

Cementation and microfossils raise s_u, while macropores keep the water content and LI high and the s_{ur} low. This is revealed in the ease and speed of manually remoulding these soils by squeezing in comparison with the others studied in the PS.

The SRD soil microstructure is disoriented, flocculated and macroporous. It has mixtures of clay matrix, some mineral grains of silt or fine sand size, and the diatom microfossils distributed throughout the sample, which can be seen only by their contours and intra-skeletal pores with elongated disk shape. Several small white particles are also observed, indicating the distribution of illite clay and cementation with iron oxide naturally present in the composition of the diatomaceous earth used. Intra-skeletal pores are numerous and close together. The macropores are spontaneously cemented and interconnected in such a way that they create a skeletal framework that supports the larger inter-aggregate macropores, forming caves.

Considering that the SRD was prepared from reconstituted mud conditions and was not sedimented, it is observed that the sizes of its largest macropores are smaller than those observed in the natural diatomaceous soils of Port of Santana. On the other hand, more porosity is observed in the clayey matrix in the SRD, since it experienced lower effective vertical stress than the natural soils in the field. This sample, as well as the PS 1A 38 m, highlighted the essential role of diatom microfossils in the structural metastability of the reconstituted soil. Cementation and microfossils increase s_u, while macropores keep the water content and liquidity index high.

Porosity results extracted from the micro-CT segmented pore networks (visible pores larger than 0.9 μm) are shown in Table 4. Comparing them with the porosities obtained by the physical indices, a difference of approximately 30 % represents the micro and mesoporosity that is not contemplated by the image. Therefore, the segmented porosity represents only the macropores that influence the metastability.

Table 4. Experimental and micro-CT porosity results.

Specimens	**TEST / PROCESSING**	
	Physical index	**Micro-CT + ImageJ**
	Porosity (%)	Porosity > 0.9 μm (%)
PS 1A 36 m	59.2	31.3
PS 1A 38 m	68.3	38.5
SRD	61.5	34.3

5. Conclusions

The result of this research shows the fundamental role of diatom microfossils in pore size distribution and microstructural metastability, impacting the high sensitivity measured in soil reconstituted with diatoms (SRD) and in natural diatomaceous soils of Port of Santana (PS). Microfossils create a solid cemented and flocculated framework that elevates s_u, and with interconnected pore channels that keep the water content and liquidity index high and the s_{ur} low.

Finally, it is concluded that the diatom microfossils present in the Port of Santana natural soils and the SRD are responsible for maintaining high moisture and liquidity indices, even at great depths or under high geostatic effective stresses, since they are largely responsible for the physical-chemical structuring of the soil and store non-adsorbed water in their pores. This free water is suddenly released if the soil undergoes undrained disturbance. Then, the metastable structure created by microfossils collapses abruptly, assuming undrained remoulded strength, s_{ur}, and the ruptured soil behaves like a viscous fluid, which allows flowslide to occur in the field.

Acknowledgements

This work was developed as part of the PRONEX research project E-26/210.920/2016 (209429) financed by the Rio de Janeiro State (FAPERJ) and the Brazilian State (CNPq) research supporting agencies. The first author acknowledges the support of the Coordination of Improvement of Higher Education Personnel - Brazil (CAPES) - Code of Financing 001.

The authors also acknowledge SEA and Anglo American for providing the Shelby samples and the fall cone and SEM test results on the soil of Port of Santana. Thanks area also due to professors Ian Schumann and Michel Tassi, for helping to carry out laboratory vane tests at the Geotechnical Laboratory of COPPE-UFRJ and professors Janine Vieira and Rodrigo Raposo of the Micro-CT Laboratory at UFF for supporting the execution of X-ray micro-CT of soils.

References

Arganda-Carreras, I., Kaynig, V., Rueden, C., Eliceiri, K. W., Schindelin, J., Cardona, A., Sebastian Seung, H. “Trainable Weka Segmentation: a machine learning tool for microscopy pixel classification”, Bioinformatics, 33(15), 2424–2426, 2017. doi:10.1093/bioinformatics/btx180

Barreto, E. C. G. “Physical, chemical, mineralogical and microstructural characterization of the soft soil involved in the failure at the Port of Santana”, MSc Dissertation in Portuguese, Pontifical Catholic University of Rio de Janeiro, 207 pages, 2015.

Barreto, E. C. G. “Evaluation of the influence of the presence of diatom microfossils on the development of high sensitivity clays”, DSc Thesis in Portuguese, Pontifical Catholic University of Rio de Janeiro, 279 pages, 2021.

Collins, K., McGown, A. “The form and function of microfabric features in a variety of natural soils”, Geotechnique 24 (2), 223–254, 1974.

Delage, P., Lefebvre, G. “Study of the structure of a sensitive Champlain clay and of its evolution during consolidation”, Canadian Geotechnical Journal, 21, 21-35, 1983.

Diamond, S. “Pore size distribution in clays”, Clays and Clay Minerals 18, 7–23, 1970.

Hong, Z., Tateishi, Y., Han, J. “Experimental study of macro and micro-behavior of natural diatomite”, J Geotech Geoenviron Engng ASCE 132, No. 5, 603–610, 2006.

Landis, E. N., Keane, D. T. “X-ray Microtomography”, Materials Characterization, 61, 1305-1316, 2010.

Lebuis, J., Robert, J. M., Rissman, P., “Regional mapping of landslides hazard in Quebec”In: Proc Symposium on Slopes in Soft Clays, Linköping, SGI Report No. 17: 205-262, 1983.

Locat, J., Tanaka, H. “Glacial and non-glacial clays: nature and microstructure of selected clays”, In: Proceedings IS-Yokoham of Soft Sediments, 2000.

Locat, J., Tanaka, H. “A new class of soils: Fossiliferous soils?”, In: Proc Fifteenth Int Conf on Soil Mechanics and Geotechnical Engineering, 3, 2295– 2300, 2001.

Rietveld, H. M., Acta Crystallogr., 21, A228, 1966.

Sandroni, S. S., Leroueil, S., Barreto, E. C. G. “The Santana Port accident: Could it be a sensitive clay flowslide under the Equator?”, In: GeoQuebec Canadian Geotechnical Conference, Quebec, Canada, 2015.

Sasanian, S., Newson, T. A. “Use of mercury intrusion porosimetry for microstructural investigation of reconstituted clays at high water contents”, Engineering Geology, 158, 15–22, 2013.

Skempton, A. W., Northey, R. D. “The sensitivity of clays”, Geotechnique, 3, 30-53, 1952.

Staniewicz, L., Midgley, P. A. “Machine learning as a tool for classifying electron tomographic reconstructions”, Advanced Structural and Chemical Imaging, 1:9, 2015. doi 10.1186/s40679-015-0010-x

Tanaka, H., Locat, J. “A microstructural investigation of Osaka Bay clay: The impact of microfossils on its mechanical behaviour”, Canadian Geotechnical Journal, 36, 3, 493–508, 1999.

Tanaka, H., Locat, J., Shibuya, S., Soon, T.T., Shiwakoti, D. R. “Characterization of Singapore, Banghok, and Ariake clays”, Canadian Geotechnical Journal 38 (2): 378-400, 2001.

Tanaka, H., Hirabayashi, H., Matsuoka, T., Kaneko, H. “Use of fall cone test as measurement of shear strength for soft clay materials”, Soils and Foundations 52 (4), 590-599, 2012.

Washburn, E. W. “Note on a method of determining the distribution of pore sizes in a porous material”, In: Proceedings of the National Academy of Sciences of the United States ofAmerica 7 (4), 115–116, 1921.